Proceedings of the 2011 6th IEEE International
Conference on Nano/Micro Engineered and Molecular Systems
February 20-23, 2011, Kaohsiung, Taiwan

Fractal Grooves Applied to Passive Micro-Mixers

A-Fu Kao, Lung-Jieh Yang*, *Member, IEEE,* Fu-Wen Yeh

***Abstract*—The purpose of the present work is to study on the application of a navel fractal pattern to passives micro-mixers. The SU-8 soft lithography is used to transfer the fractal grooves and the micro channel to PDMS mold on a glass. The authors also used numerical software Fluent to simulate the flow fields of the new passive micro-mixers. The 3 kinds of fractal configurations, three flow conditions (Re=0.64, 6.4, and 64) have been compared with the experimental mixing indices. The simulation results show that the novel fractal pattern do create lateral mass transport to improve mixing. With the same fractal patterns, the lower Reynolds number flow (0.64) has the higher mixing index. The branch with fractal patterns for two times (type III) is also better than other cases with high mixing performance.**

***Index Terms*—soft lithography, fractal, passive micro-mixer**

I. Introduction

In recent years, the micro-mixers which have attracted attention become a very popular topic in microfluidics. As being classified to passive and active types by their respective working principles [1], the passive micro-mixer has the advantages of simple structure, low cost, and easy manufacture. How to improve the mixing performance of them in a very confined space is the most concerned issue. Strook et al. [2] constructed a passive micro-mixer using staggered herringbone structures to produce chaotic flows to improve the mixer performance. Chaotic advection is the main characteristic of their micro-mixer. Aref [3] also introduced the development of chaotic advection. In general, the flow channel geometry is the key factor to conduct the performance of passive micro-mixer, so many researchers have made effort to the novel configurations such as Y-channel [4], three-dimensional serpentine micro-channel [5], Tesla structures [6], and T-mixer [7].

II. Micromixer design

Yang et al. [8] found a tree-like, dendrite, fractal micro structures in gelatin as Fig. 1. These fractal patterns may have the emerging application to new chaotic micro-mixer design. However, the fractal pattern is too complicate to analyze. So, the present paper proposed new fractal patterns inspired by Fig. 1. Three tree-like fractal patterns have been designed. They are with branches for one time (type II), two times (type III), and three times (type IV). The schematic diagrams are shown in Fig. 2. The passive micro-mixers are embedded with fractal grooves on the bottom surface to improve the mixing. The micro-mixer with no fractal pattern, type I, is fabricated as the baseline device for performance comparison. The fractal dimensions (D_b) are also calculated, by the box theory [9], as Eq. (1),

$$D_b = \lim_{s \to 0} \frac{\ln N(s)}{\ln(\frac{\ell}{s})} \quad (1)$$

where $N(s)$ denotes the box number of the area that covers the fractal patterns in the whole image, s denotes the width of the small box, and ℓ denotes the length of the whole image. D_b of type II, type III, and type IV are 1.222, 1.585, and 1.716, respectively, in Table 1. The fractal dimension is useful in categorizing the geometry characteristic of the fractal grooves in the design of new chaotic micro-mixers comparable to the prior art [2].

III. Methods and discussions

A. Fabrication and performance test

The soft lithography is used to fabricate the micro-mixer. The SU-8 mixer patterns are transferred to PDMS molds and then bonds the PDMS molds with cover glasses [10-11]. The fabrication process is shown in Fig. 3. The actual device of the PDMS micro-mixer is shown in Fig. 4. There are two holes as the inlet and outlet on each end of the PDMS device. Experimental setup for characterizing mixing performance is as Fig. 5. An inverted fluorescence microscopy is used to capture the mixing image of the microchannel, and the mixing performance is evaluated by image processing afterwards.

B. Numerical simulation

The numerical software Fluent is also applied to simulate the passive micro-mixers. To minimize effects of mesh on mixing efficiency, the mesh size has been tested. The computational domain was discretized with unstructured cells, around 440,000 cells per types. A close-up view of the mesh near the tree-fractal pattern is shown in Fig. 6. The simulation environment was defined for steady incompressible flows. The physical properties of water were applied to the two fluids in the simulation, a diffusion coefficient of $1.2 \times 10^{-9} m^2 s^{-1}$ was used for all the simulations. The boundary condition of inlet was set to a fixed-velocity as well as the outlet was set to 1 atmospheric pressure. The mass fraction of the up-inlet fluid species was set to 1 (red color) and the down-inlet to 0 (blue color) to define the mixing condition. As mixing takes place the mass fraction of up side of the channel decrease from 1, while the down side

A-Fu Kao: Post doctor researcher, Department of Mechanical and Electromechanical Engineering, Tamkang University, 151 Ying-chuan Rd., Tamsui, 25137, Taipei County, Taiwan.
*Lung-Jieh Yang: Professor, Department of Mechanical & Electromechanical Engineering, Tamkang University, Tamsui, 25137 Taiwan (corresponding author to provide phone: +886-932159193; fax: +886-2-26209745; e-mail: Ljyang@mail.tku.edu.tw).
Fu-Wen Yeh: Master research with the corresponding author.

978-1-61284-777-1/11/$26.00 ©2011 IEEE

increases from 0. Complete mixing was achieved when the mass fraction of the two fluids reach 0.5 (green color).

C. Results and discussion

Three fractal grooves (Fig. 2) have been placed on the channel to be studied about their effect on mixing performance. Fig. 7 shows the mass fraction contour of numerical simulation at Z=10μm of type II. The main stream velocity is 6.5 mm/sec (Re=0.64). The inlet of the mixer is at the left side. From the picture, we find the mixing performance increasing as the fluid passing the fractals due to the fractal generates chaotic advection and diffusion effects to stir the flow and induce fluidic mixing. Fig. 8 shows the mass fraction contours of type III and has the same behavior as Fig. 7. The number 1 stands for the rear region of the 1st fractal in the channel. The number 2 and 3 represent the same area of the 2nd and 3rd fractals, respectively.

Mass fraction distributions of vertical cross sections at the interaction position and around the three fractals of type III, Re=0.64 are shown in Fig. 9. The close-up views of the cross section are magnified in Fig. 10. The red and blue represent the low mixing performance, green mixing means the complete mixing. There are three vertical cross sections at Fig. 10(1). It can be seen that the center green region is growing as approaching to downstream. If we focus on the left blue area of the 3rd vertical section, there is a light blue at the corner near the groove. This is due to the oblique grove leads the other side fluid to here. The orange color has shown at the red edge too. That means the tree like groove works to improve the mixing performance. Comparing Figs. 10(1), 10(2), and 10(3), the center green region is growing as well as the red and blue regions shrinking. Especially at the end section in Fig. 10(3), the pure blue and red almost vanish.

To understand the detail mixing behavior, the mass fraction distribution at the end region of the three fractals of type II and type III were shown in Figs. 11 and 12, respectively. The good mixing criteria depend on the difference of the mass fraction profile from a step profile (no mixing case.) Additionally, a good mixing also depends on the mass fraction getting near to 0.5 or not. With the above guidelines, we compared the three distribution lines at y=0.25mm and found that the left-side mass fraction of No. 3 is the smallest. Meanwhile, the right-side mass fraction of No. 3 is reversely the biggest. That means the mixing performance at region No. 3 is the best over other two regions. The reason for the above mixing result is that No.3 is at the most downstream position in the mixer device.

Fig. 13 shows the fluorescent micrographs of horizontal cross sections of micro-mixers. The flow direction is from left to right so the fractal has a divergent effect to fluid. The configurations of (a), (b), (c) and (d) are type I, type II, type III, and type IV, respectively. The up-left picture of Fig. 13(b) is at the entrance, so the two fluids separate clearly. The up-right picture of Fig. 13(b) is at the first fractal (No. 1) region. It's easy to find that there is a bit fluorescent fluid from up to low. The down-left and down-right pictures are at No. 2 and No. 3 region respectively. As the region move to downstream, there is more fluorescent fluid conducted by the fractal groove to transport laterally. The flow in Figs. 13(c) and 13(d) also behave the same manner. The mixing index values defined as Eq. (2) are derived from the mixing images, not show here all, by MATLAB and summarized in Table 2.

$$M_I = 1 - \frac{1}{\bar{I}}\sqrt{\frac{\sum_{j=1}^{N}\left(I_j - \bar{I}\right)^2}{N}} \qquad (2)$$

where I_j and $\bar{I}$ denotes the image grayscale of the pixel j and the average grayscale; N are the total number of the image pixels. The mixing index M_i basically increases as Re decreases subject to all testing micro-mixers. Additionally, for the better cases subject to Re=0.64, the fractal patterns with branch two times (type II), instead of the three times (type III), has the highest mixing index among the test cases. The detailed reason is still under investigation.

IV. Conclusion

The paper shows a novel passive micro-mixer which placed a tree like fractal grooves on the channel. Both of MEMS technology and numerical simulation have been applied to the research. In addition to the blank mixer, three types of micro-mixers with tree like fractal of branch of one, two, and three times were investigated. To create lateral mass transport to improve mixing, the tree like fractal pattern is laid on the channel bottom surface. With the same fractal patterns, the lower Reynolds number flow (0.64) has the higher mixing index. The fractal patterns branch for two times (type III) is also better than other cases with high mixing performance.

Acknowledgement

Funding for this work was provided by the National Science Council of Taiwan with the project no. of NSC-98-2221-E-032-025-MY3 and NSC-98-2221-E-032-049. The authors are also grateful to Professor H. J. Sheen and Dr. C. J. Lee of Institute of Applied Mechanics, National Taiwan University for their support of inverted microscopy facilities.

References

[1] N. T. Nguyen and Z. Wu, "Micromixers– a review," *Journal of Micromechanics and Microengineering*, vol. 15, no. 2, pp. R1-R16, 2005.

[2] A. D. Stroock, S. K. W. Dertinger, A. Ajadari, I. Mezic, H. A. Stone, and G. M. Whitesides, "Chaotic mixer for microchannels," *Science*, vol. 295, pp. 647-651, 2002.

[3] H. Aref, "The development of chaotic advection," *Physics of Fluids*, vol. 14, no. 4, pp. 1315-1325, 2002.

[4] H. Wang, P. Iovenitti, E. Harvey, and S. Masood, "Optimizing layout of obstacles for enhanced mixing in microchannels," *Smart Materials and Structures*, vol. 11, no. 5, pp. 662-667, 2002.

[5] R. H. Liu, M. A. Stremler, K. V. Sharp, M. G. Olsen, J. G. Santiago, R. J. Adrian, H. Aref, and D. J. Beebe, "Passive mixing in a three-dimensional serpentine microchannel," *Journal of Microelectromechanical Systems*, vol. 9, no. 2, pp. 190-197, 2000.

[6] C. C. Hong, J. W. Choi, and C. H. Ahn, "A novel in-plane passive microfluidic mixer with modified Tesla structures," *Lab on a Chip*, vol. 4, no. 2, pp. 109-113, 2004.

[7] S. H. Wong, M. C. L. Ward, and W. Wharton, "Micro T-mixer as a rapid mixing micromixer," *Sensors and Actuators B: Chemical*, vol. 100, pp. 359-379, 2004.

[8] L. J. Yang, C. C. Le, P. H. Chen, and C. W. Hsu, "Confined fractal patterns in gelatin," Proc. of the 6th IEEE-NEMS conference, Kaohsiung, Taiwan, 2011.
[9] Y. Q. Hu, Y. P. Zhao, and T. X. Yu, "Fractal pattern formation in anodic bonding of Pyrex glass/Al/Si," *International Journal of Nonlinear Sciences and Numerical Simulation*, vol. 9, no. 4, pp. 315-322, 2008.
[10] J.-M. Wang and L.-J. Yang, "Electro-hydro-dynamic (EHD) micropumps with electrode protection by parylene and gelatin," *Tamkang Journal of Science and Engineering*, vol. 8, no. 3, pp. 231-236, 2005.
[11] B. H. Jo, L. M. Van Lerberghe, K. M. Motsegood, and D. J. Beebe, "Three-dimensional micro-channel fabrication in polydimethylsiloxane (PDMS) elastomer," *Journal of Microelectromechanical Systems*, vol. 9, no. 1, pp. 76-81, 2000.

Table 1. The configurations of the testing micro-mixers

Type	I	II	III	IV	Ref. [2]
Patterns branch times	0	1	2	3	Herring bone
Fractal dimension; D_b (by box theory)	0	1.222	1.585	1.716	1.87

Table 2. Mixing index of the micro-mixers

Re	Convergent Branch time=1	Converge nt Branch times=2	Convergent Branch times=3	Divergent Branch time=1	Divergent Branch times=2	Divergent Branch times=3
0.64	60%	56%	58%	64%	67%	58%
6.40	52%	55%	53%	55%	60%	55%
64.0	50%	52%	52%	46%	46%	47%

Fig. 1. *Classical* fractal micro patterns in the $K_2Cr_2O_7$-gelatin collagen matrix [8].

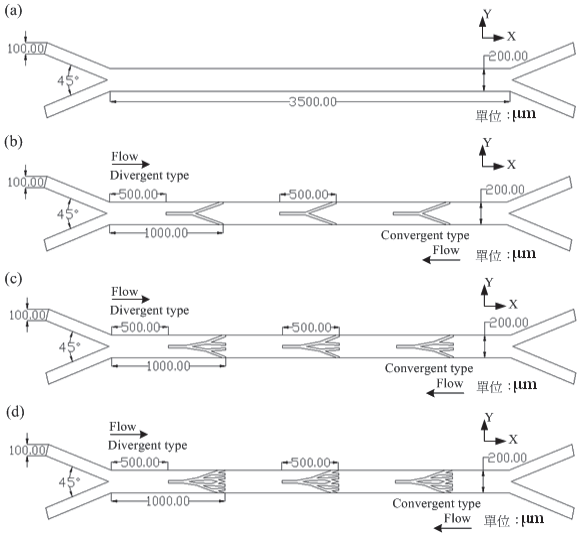

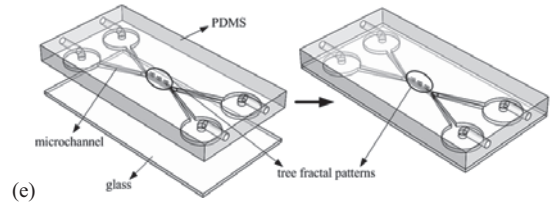

Fig. 2. Schematic diagrams of the new micro-mixers: (a) type I, (b) type II, (c) type III, (d) type IV, (e)the whole configuration.

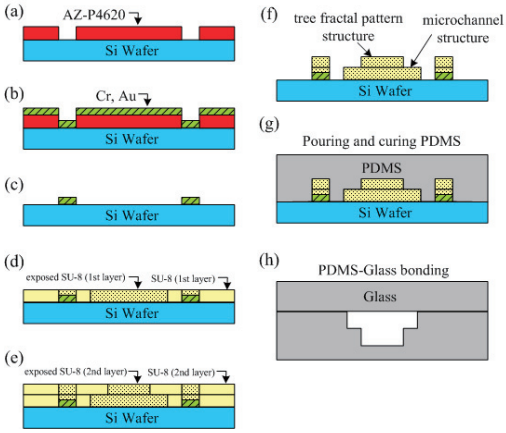

Fig. 3. Illustration of the fabrication process for micro-mixer: (a-c)Cr/Au alignment mark by lift-off; (d)1st exposure of SU-8; (e)2nd exposure of SU-8; (f)developing the SU-8; (g)PDMS molding/de-molding; (h)bonding the PDMS mold with the glass substrate.

Fig. 4. Photograph of an actual PDMS device for mixing experiments.

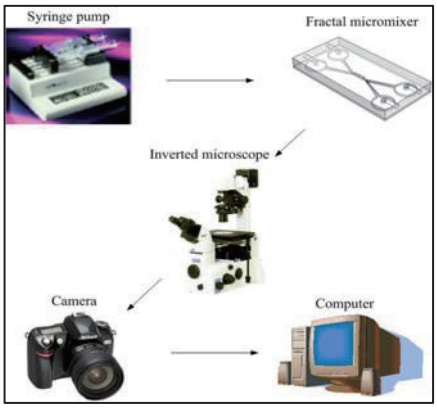

Fig. 5. Experimental setup for characterizing micro-mixer performance

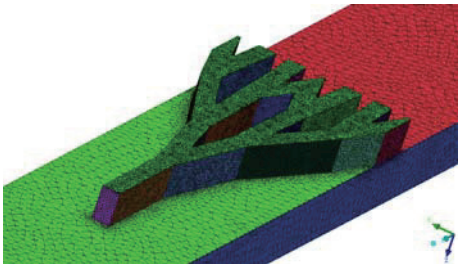

Fig. 6. Close-up illustration of meshes around the fractal(Type III) on the back of micro-channel.

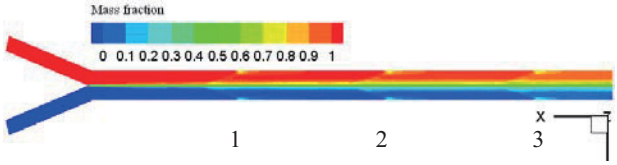

Fig. 7. Mass fraction contour at Z=10μm of type II, Re=0.64. The numbers, 1, 2, and 3 stand for the three fractals on the bottom of the mixer.

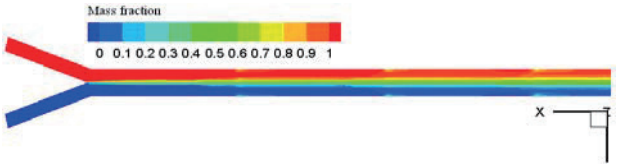

Fig. 8. Mass fraction contour at Z=10μm of type III, Re=0.64.

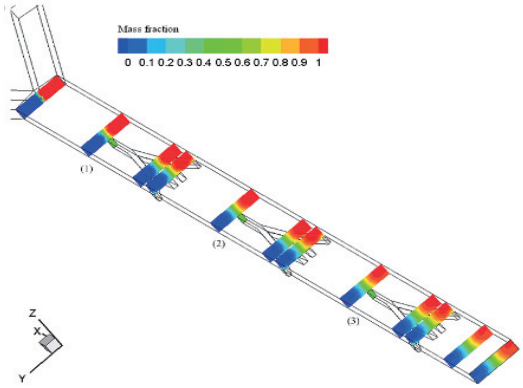

Fig. 9. Mass fraction contours of vertical cross sections at the interaction position and around the three fractals of type III, Re=0.64. The numbers indicate the fractal on the channel bed.

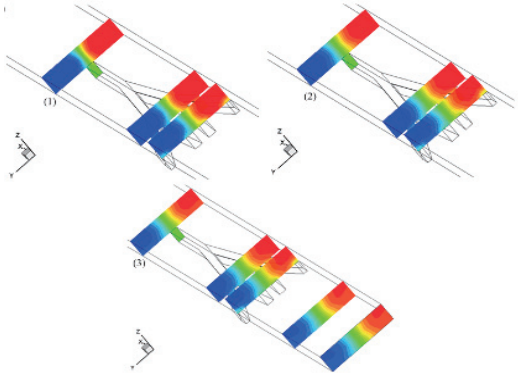

Fig. 10. Close-up views of vertical cross section of Fig. 9. (1) the 1st fractal, (2) the 2nd fractal, (3) the 3rd fractal.

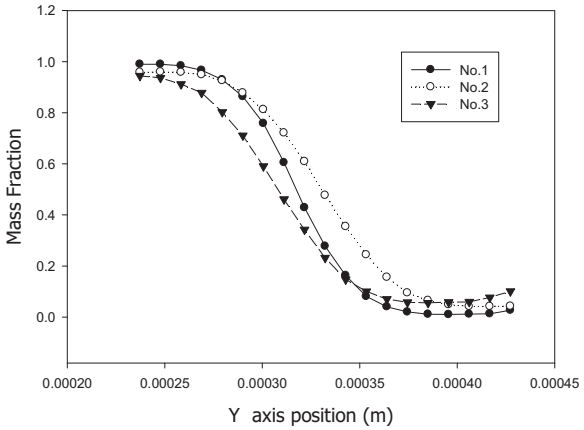

Fig. 11. Mass fraction distribution at the different points of type II fractal (the numbers 1-3 identical to Fig.7.)

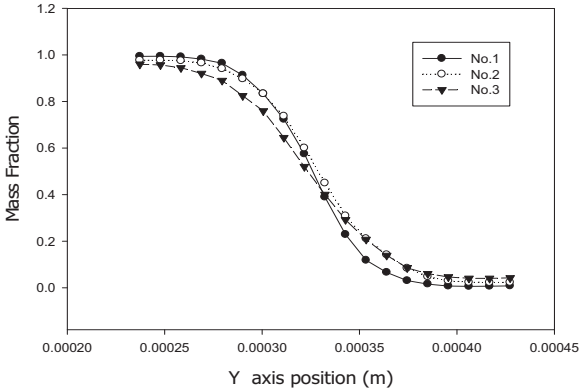

Fig. 12. Mass fraction distribution at the different points of type III fractal (the numbers 1-3 identical to Fig.7.)

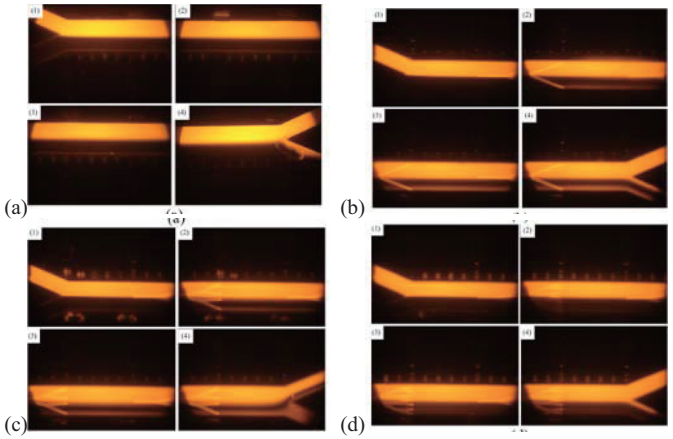

Fig. 13. Fluorescent micrographs of horizontal cross sections of micro-mixers, flow direction from left to right: (a) type I; (b) type II; (c) type III; (d) type IV.